

Quantum and Thermal Phase Transitions in a Bosonic Atom-Molecule Mixture in a Two-dimensional Optical Lattice

L. de Forges de Parny^{1,2} and V.G. Rousseau³

¹ *Laboratoire de Physique, CNRS UMR 5672, École Normale Supérieure de Lyon, Université de Lyon, 46 Allée d'Italie, Lyon, F-69364, France*

² *Physikalisches Institut, Albert-Ludwigs Universität Freiburg, Hermann-Herder Straße 3, D-79104, Freiburg, Germany and*

³ *Physics Department, Loyola University New Orleans, 6363 Saint Charles Ave., New Orleans, Louisiana 70118, USA*

(Dated: January 9, 2017)

We study the ground state and the thermal phase diagram of a two-species Bose-Hubbard model, with $U(1) \times \mathbb{Z}_2$ symmetry, describing atoms and molecules on a two-dimensional optical lattice interacting via a Feshbach resonance. Using quantum Monte Carlo simulations and mean field theory, we show that the conversion between the two species, coherently coupling the atomic and molecular states, has a crucial impact on the Mott-superfluid transition and stabilizes an insulating phase with a gap controlled by the conversion term – the *Feshbach insulator* – instead of a standard Mott insulating phase. Depending on the detuning between atoms and molecules, this model exhibits three phases: the Feshbach insulator, a molecular condensate coexisting with noncondensed atoms and a mixed atomic-molecular condensate. Employing finite-size scaling analysis, we observe three-dimensional (3D) XY (3D Ising) transition when $U(1)$ (\mathbb{Z}_2) symmetry is broken whereas the transition is first-order when both $U(1)$ and \mathbb{Z}_2 symmetries are spontaneously broken. The finite temperature phase diagram is also discussed. The thermal disappearance of the molecular superfluid leads to a Berezinskii-Kosterlitz-Thouless transition with unusual universal jump in the superfluid density. The loss of the quasi-long-range coherence of the mixed atomic and molecular superfluid is more subtle since only atoms exhibit conventional Berezinskii-Kosterlitz-Thouless criticality. We also observe a signal compatible with a classical first-order transition between the mixed superfluid and the normal Bose liquid at low temperature.

PACS numbers: 03.75.Hh, 05.20.y, 05.30.Jp, 64.60.F-, 03.75.Mn

I. INTRODUCTION

Ultracold atoms in optical lattices have opened new perspectives in several modern fields of physics, such as many-body and condensed matter physics. They offer possibilities to study complex many-body systems [1] and quantum phase transitions [2, 3] with a high degree of control. More interestingly, they are quantum simulators, giving access to the experimental implementation of models which are not easily realizable in any other physical contexts. In all these applications, Feshbach resonances offer an invaluable tuning knob for controlling the interaction between the atoms [4] and also give the possibility of coherently coupling different internal states of atoms. As an example, an unbound state of two interacting atoms and a bound state – hereafter called the *molecular state* – can be brought into resonance by the application of a magnetic field, thanks to the different magnetic moments of the two states. Therefore, ultracold atoms in optical lattices are also very suitable to study mixtures of Bose-Einstein condensates (BECs), involving a coherent coupling *à la* Josephson between pairs of atoms and molecules – realizing quantum-coherent chemical reactions. The control of the effective scattering length of unbound atoms has led to the exploration of complex quantum many-body phases [4–11] and to tune transitions between them [12, 13], whereas the control of the coherent coupling between atoms and molecules has

been exploited e.g. to observe atom-molecule Rabi oscillations [14–16]. Theoretically, the coherent coupling is at the basis of the prediction of a quantum phase transition between mixed atom-molecule and purely molecular condensates [17–25]. The case of bosonic atoms and molecules is all the more interesting since long-range phase coherence can be established in two dimensions at zero temperature via Bose-Einstein condensation. The asymmetric coherent coupling between atoms and molecules clearly leads to a complex interplay between atomic and molecular condensations and provides quantum phase transitions which are not realized in the context of single species condensates. Even more striking is that the coherent coupling can destroy the phase coherence, leading to an insulating phase with a gap controlled by the conversion amplitude [21].

In this paper we focus our attention on the case of a two dimensional (2D) atom-molecule mixture using quantum Monte Carlo (QMC) simulations and Gutzwiller mean field theory (MFT). Our goal is twofold: we elucidate the effect of the conversion term, leading to a rich and original ground state phase diagram and we unveil the thermal phase transitions, exhibiting an unusual Berezinskii-Kosterlitz-Thouless (BKT) transition. Basically, we expect mixed Mott insulator and superfluid phases, i.e., composed by both atoms and molecules, to appear due to the conversions. However, the effect of conversions on the phase transitions is more subtle and

we report here a clear evidence that the phase coherence is destroyed when the conversion amplitude is increased. Indeed, close to the resonance, the conversion term has a crucial impact on the Mott-superfluid transition for two particles per site: it enhances the insulator phase and also changes the nature of the transition, leading to a quantum first-order transition with a $U(1) \times \mathbb{Z}_2$ symmetry breaking. Even more interestingly, the phase located at the tip of the insulating lobe with two particles per site in the phase diagram does not correspond anymore with the definition of a Mott insulator phase, i.e an insulating phase with a particle-hole gap opened by (diagonal) repulsive interactions between the particles [26]. Instead of this, the system adopts a Feshbach insulating phase where the energy gap is controlled by the (off-diagonal) conversion term between atoms and molecules, keeping the interactions fixed. Although the existence of this phase was previously reported in Ref. [21], our present study provides a reliable analysis of the quantum phase transitions, completing the characterization of the phase diagram. Finally, we study the thermal phase transitions. In two dimensions, Bose-Einstein condensation at finite temperature is impossible in the proper sense, leaving space to quasicondensation via a BKT transition [27]. The atomic and molecular conversions induce an asymmetric coupling between the phase of the atomic and molecular wave functions which couples the topological excitations (vortex-antivortex pairs) of both fields. For positive detuning, this leads to an unusual BKT transitions when the quasi-long-range coherence of the mixed atomic and molecular superfluid is destroyed: only atoms exhibit conventional BKT criticality whereas molecules quasicondense in the same way as atom pairs condense. Our QMC simulations are in agreement with a previous study of an effective XY coupled model, mimicking the atomic and molecular superfluid for positive detuning [28]. We complete here the picture by studying the thermal transition for negative detuning: the molecular condensate, coexisting with noncondensed atoms, exhibits conventional BKT criticality but is found to be consistent with an anomalous stiffness jump at the transition.

The paper is organized as follows: The atom-molecule Hamiltonian is presented in Sec. II. In Sec. III, we discuss the mean field and quantum Monte Carlo approaches used to study the Hamiltonian. We also define the main observables of interest. Section IV is devoted to the discussion of the ground state phase diagram. Quantum Monte Carlo calculations verify the qualitative conclusions of the mean field theory, but provide quantitatively accurate values for the phase boundaries and elucidate the universality classes of the quantum phase transitions. Finally, in Sec. V, we discuss the thermal phase diagram and the nonconventional BKT transitions associated with the loss of molecular and atomic-molecular quasi-long-range coherence. Conclusions and outlook are provided in Sec. VI.

II. ATOM-MOLECULE HAMILTONIAN

We consider spinless bosons with mass m on a square optical lattice close to a narrow Feshbach resonance. The system is described by a single-band Bose-Hubbard model with atomic and molecular bosons, coherently coupled via atom-atom interactions [29]. The particles can hop between nearest neighboring sites, and their interactions are described by intraspecies and interspecies on-site potentials. An additional term takes into account the conversion between two atoms and a molecule, and vice versa. The Hamiltonian of the system reads [17–19, 29, 30] $\hat{\mathcal{H}} = \hat{\mathcal{T}} + \hat{\mathcal{P}} + \hat{\mathcal{C}}$, where

$$\hat{\mathcal{T}} = - \sum_{\langle i,j \rangle} \left(t_a a_i^\dagger a_j + t_m m_i^\dagger m_j + \text{H.c.} \right), \quad (1)$$

$$\begin{aligned} \hat{\mathcal{P}} = \sum_i & \left[\frac{U_a}{2} n_i^a (n_i^a - 1) + \frac{U_m}{2} n_i^m (n_i^m - 1) \right. \\ & \left. + U_{am} n_i^a n_i^m + (U_a + \delta) n_i^m - \mu (n_i^a + 2n_i^m) \right], \end{aligned} \quad (2)$$

$$\hat{\mathcal{C}} = g \sum_i \left(m_i^\dagger a_i a_i + a_i^\dagger a_i^\dagger m_i \right). \quad (3)$$

The $\hat{\mathcal{T}}$ operator corresponds to the kinetic energy for hopping between nearest neighboring sites $\langle i, j \rangle$ defined on a $L \times L$ square lattice with periodic boundary conditions. Here t_a and t_m are respectively the tunneling amplitudes for the atoms and the molecules. The a_i^\dagger and a_i (m_i^\dagger and m_i) operators are bosonic creation and annihilation operators of atoms (molecules) on site i . $n_i^a = a_i^\dagger a_i$ and $n_i^m = m_i^\dagger m_i$ are the corresponding number operators. The $\hat{\mathcal{P}}$ operator contains the intraspecies (interspecies) interactions with repulsive cost U_a and U_m (U_{am}), as well as the chemical potential term; in particular it contains the detuning term δ (controlled experimentally by a magnetic field [4]), which brings the state of two atoms and a molecule in and out of resonance on each site, $\delta < 0$ ($\delta > 0$) corresponding to the molecular (atomic) side of the resonance. Finally the $\hat{\mathcal{C}}$ operator is the conversion term, which coherently transforms a pair of atoms into a molecule and vice versa [20]. The conversion rate between atoms and molecules, g , is obtained via the solution of the scattering problem for two atoms in a parabolic potential [15]. Following Ref. [14], the parameter g , calculated by assuming a single harmonic potential, which is a good approximation for a deep optical lattice, is given by

$$g = \left[\frac{4\pi\hbar^2 a_{\text{bg}} \Delta\mu \Delta B}{m(\sqrt{2\pi} a_{\text{ho}})^3} \left(1 + 0.490 \frac{a_{\text{bg}}}{a_{\text{ho}}} \right) \right]^{\frac{1}{2}}, \quad (4)$$

where $a_{\text{ho}} = \sqrt{\hbar/m\omega}$ the harmonic oscillator length, a_{bg} the background scattering length of the atoms, ΔB the width of the Feshbach resonance, and $\Delta\mu$ the difference between the magnetic moments of an entrance-channel atom pair and a closed-channel molecule. The model described by the Hamiltonian $\hat{\mathcal{H}}$ remains realistic as long as

$t_a, t_m, |V_{aa}| \ll \hbar\omega$, with V_{aa} the nonresonant atom-atom interaction and $\hbar\omega$ the energy splitting of the on-site optical lattice potential; see Ref. [29] for the conditions of applicability of this model and for the derivation of the Hamiltonian Eqs. (1–3) from a microscopic model. Furthermore, the validity of the single-band approximation requires $\sqrt{2}a_{\text{bg}}\Delta\mu\Delta B/a_{\text{ho}} \ll \hbar\omega$. In other words, the single-band approximation is well respected for a narrow Feshbach resonance, e.g. $\Delta B = 15$ mG for ^{87}Rb near 414 G [14].

The Hamiltonian $\hat{\mathcal{H}}$ has the symmetry $U(1) \times \mathbb{Z}_2$, associated with the mass conservation in the mixture ($U(1)$ symmetry), times the Ising \mathbb{Z}_2 symmetry in the phase relationship between atoms and molecules. As we discuss later, this emergent Ising symmetry, arising from the asymmetric nature of the atom-molecule coupling, is crucial for the understanding of the phase diagram. A theoretically sound treatment requires one to take into account the full many-body physics of the Hamiltonian $\hat{\mathcal{H}}$ which is a rather hard task, given the large number of parameters ($t_a, t_m, U_a, U_m, U_{am}, \mu, \delta, g$). In order to simplify our study, we treat the parameters of the model as free parameters and we consider symmetric parameters for atoms and molecules, leading to

$$\begin{aligned} t &\equiv t_a = t_m, \\ U &\equiv U_a = U_m = U_{am}, \end{aligned} \quad (5)$$

reducing the number of parameters to four independent parameters only: $t/U, \delta/U, \mu/U$ and g/U , where we choose the hopping parameter $t = 1$ in order to set the energy scale. A realistic scenario requires the calculation of the parameters from the microscopic Hamiltonian using the Wannier functions. Nevertheless, since the qualitative aspects of the phase diagram do not depend on the precise values of $g, U_a/U_m$ and t_a/t_m , our choice of Eq. (5) is indeed relevant [17] and captures the physics arising from the conversion term Eq. (3), which is demonstrated in Ref. [21].

The above atom-molecule Hamiltonian has been mainly studied using mean-field theory [18–20]. The quantum phase transitions exhibited by the model have been extensively studied in one dimension [24, 25, 31, 32] whereas few studies have examined this question in two dimensions [17, 21]. Here we numerically investigate this Hamiltonian in two dimensions, by using exact QMC simulations based on the stochastic Green function algorithm [33, 34] and Gutzwiller mean field approach. We investigate both the quantum and thermal phase transitions.

III. METHODS

To capture the zero-temperature physics of the model, we use both the QMC method and the MFT approach. While the QMC simulations become rather demanding for the calculation of the phase diagram, MFT allows for

a rapid reconstruction of the phase boundaries, which turns out to be essential given the rich structure of the phase diagram - containing different critical and multicritical points.

A. Gutzwiller mean-field approach

Although the mean field approximation does not give quantitatively accurate values for the phase boundaries, the mean-field phase diagram of a bosonic coupled mixture is in good agreement with QMC simulations in two dimensions at zero temperature [35, 36] but fails at finite temperature [37]. We use a mean-field formulation based on a decoupling approximation which decouples the hopping term to obtain an effective one-site problem. Introducing the atomic (molecular) superfluid order parameter $\psi_a \equiv \langle a_i^\dagger \rangle = \langle a_i \rangle$ ($\psi_m \equiv \langle m_i^\dagger \rangle = \langle m_i \rangle$), we replace the creation and destruction operators on site i by their mean values ψ_a and ψ_m . Since we are interested in equilibrium states, the order parameters can be chosen to be real. Using this ansatz, the kinetic energy terms, which are nondiagonal in boson creation and destruction operators, are decoupled as

$$\begin{aligned} a_i^\dagger a_j &= (a_i^\dagger - \psi_a)(a_j - \psi_a) + (a_i^\dagger + a_j)\psi_a - \psi_a^2 \\ &\simeq (a_i^\dagger + a_j)\psi_a - \psi_a^2. \end{aligned} \quad (6)$$

The same approximation applies for the molecules. The Hamiltonian $\hat{\mathcal{H}}$ is rewritten as a sum over local terms $\hat{\mathcal{H}} = \sum_i \hat{\mathcal{H}}_i^{MF}$ where

$$\begin{aligned} \hat{\mathcal{H}}_i^{MF} &= -4t_a(a_i^\dagger + a_i)\psi_a - 4t_m(m_i^\dagger + m_i)\psi_m \\ &\quad + 4t_a\psi_a^2 + 4t_m\psi_m^2 + U_{am}n_i^a n_i^m \\ &\quad + \frac{U_a}{2}n_i^a(n_i^a - 1) + \frac{U_m}{2}n_i^m(n_i^m - 1) \\ &\quad + (U_a + \delta)n_i^m - \mu(n_i^a + 2n_i^m) \\ &\quad + g(m_i^\dagger a_i a_i + a_i^\dagger a_i^\dagger m_i). \end{aligned} \quad (7)$$

The mean field Hamiltonian Eq. (7) can be easily diagonalized numerically in a finite occupation-number basis $\{|n_a, n_m\rangle\}$, with the truncation $n_a^{max} = n_m^{max} = 10$, and then minimizing the lowest eigenvalue with respect to the order parameters ψ_a and ψ_m . This gives the order parameters of the ground state and its eigenvector $|\Psi_0^{MF}\rangle$. At zero temperature, the system is in a Bose-Einstein condensate phase if at least one of the order parameters is nonzero and is, otherwise, in an insulating phase. The atomic and molecular condensate fraction is given by

$$C_\alpha^{MF} = |\psi_\alpha|^2, \quad (8)$$

with $\alpha = a, m$. The atomic and molecular densities are respectively defined by

$$\begin{aligned} \rho_a &= \langle \Psi_0^{MF} | a^\dagger a | \Psi_0^{MF} \rangle, \\ \rho_m &= \langle \Psi_0^{MF} | m^\dagger m | \Psi_0^{MF} \rangle. \end{aligned} \quad (9)$$

Finally, the compressibility is given by

$$\kappa = \partial\rho/\partial\mu, \quad (10)$$

with $\rho = \rho_a + 2\rho_m$ the total density.

B. Quantum Monte Carlo simulations

The atom-molecule Hamiltonian is simulated by using the stochastic Green function algorithm [33, 34], an exact QMC technique that allows canonical and grand canonical simulations of the system at zero and finite temperatures, as well as measurements of many-particle Green functions. We treat $L \times L$ lattices with sizes up to $L = 14$. An inverse temperature of $\beta t = 2L$ allows one to eliminate thermal effects from the QMC results. We mainly focus on scans at fixed total density $\rho = \rho_a + 2\rho_m$ in the canonical ensemble and calculate the average atomic and molecular densities, $\rho_a = \frac{1}{L^2} \sum_i \langle a_i^\dagger a_i \rangle$ and $\rho_m = \frac{1}{L^2} \sum_i \langle m_i^\dagger m_i \rangle$, respectively, and the condensate fraction of atoms and molecules,

$$\begin{aligned} C_a &= \frac{1}{L^4} \sum_{i,j} \langle a_i^\dagger a_j \rangle, \\ C_m &= \frac{1}{L^4} \sum_{i,j} \langle m_i^\dagger m_j \rangle. \end{aligned} \quad (11)$$

The total density ρ is conserved in canonical simulations, but individual densities ρ_a and ρ_m fluctuate due to the conversion term Eq. (3). We also calculate the superfluid density given by fluctuations of the winding number [38]

$$\rho_s = \frac{\langle (W_a + 2W_m)^2 \rangle}{4t\beta} \quad (12)$$

IV. GROUND STATE PHASE DIAGRAMS

Without coupling between atoms and molecules, i.e. $g = 0$, the symmetry of the model is $U(1) \times U(1)$ and we expect to observe an atomic (molecular) Mott insulator for small t/U and integer filling, and atomic (molecular) Bose-Einstein condensate BEC_a (BEC_m) with broken $U(1)$ symmetry for large t/U . Activating the conversion, the symmetry of the model breaks down into a global $U(1) \times \mathbb{Z}_2$ symmetry corresponding to the transformations

$$\begin{aligned} \phi_i^m &\rightarrow \phi_i^m + \theta \\ \phi_i^a &\rightarrow \phi_i^a + \frac{\theta}{2} + \frac{1}{2}(\sigma + 1)\pi, \end{aligned} \quad (13)$$

with $\sigma = \pm 1$ the Ising variable and ϕ_i^a and ϕ_i^m respectively the atomic and molecular phases of the fields. The $U(1)$ symmetry is a joint one for atomic and molecular phases, and corresponds to total “mass” conservation with density $\rho = \rho_a + 2\rho_m$. From the mean field point

of view, the average phase of the atoms acquires a finite value in the atomic BEC phase, hence $\langle e^{i\phi_i^a} \rangle \neq 0$, and consequently $\langle e^{i2\phi_i^a} \rangle \neq 0$. As a consequence, the molecular phase ϕ_i^m locked to the nonzero value acquired by the phase of atomic pairs drive the system to a joint atomic and molecular BEC (BEC_{am}), and prohibits the existence of an atomic BEC alone without a molecular condensation. The reverse is not true: because of the asymmetric nature of the atom-molecule coupling, the molecular condensation does not imply an atomic condensation and leaves out the \mathbb{Z}_2 symmetry. Indeed, the molecular condensation leads to a finite value for the average $\langle e^{i\phi_i^m} \rangle$ which couples to twice the phase of the atoms $\langle e^{i2\phi_i^a} \rangle \neq 0$ and then fixes the phase of the atoms only modulo π , i.e. $\phi_i^a = \phi_i^m/2 \pm \pi$, leading to a fluctuating ϕ_i^a with discrete fluctuations ($\pm\pi$). Therefore, for large t/U , we expect the appearance of two Bose-Einstein condensed phases: a molecular condensate BEC_m and a mixed atomic-molecular condensate BEC_{am}.

For small hopping t/U , the coupling also strongly affects the Mott insulating phases, leading to an atomic-molecular Mott insulating phase (MI_{am}). The MI_{am} phase with $\rho = 2$ is well described by an on-site wave function of the form

$$|\Psi\rangle = \alpha(\delta/U, g/U)|2, 0\rangle + \beta(\delta/U, g/U)|0, 1\rangle, \quad (14)$$

in the occupation-number basis $\{|n_a, n_m\rangle\}$. It has been shown that the particle-hole gap $\Delta_{ph}(\delta, g) = \mu_p(\delta, g) - \mu_h(\delta, g)$, where μ_p (μ_h) is the critical chemical potential to add a particle (hole) to the incompressible phase, is strongly dependent on the conversion parameter g . For a moderate hopping, the most striking feature is that the conversion parameter g can drive the system towards an insulating phase, the Feshbach insulator (FI), close to Feshbach resonance by opening a particle-hole gap in the BEC_{am} phase existing for $g/U \rightarrow 0$ [21]. In other words, the particle-hole gap vanishes in the FI phase when the conversions are suppressed, i.e. $\Delta_{ph}(\delta/U, g/U \rightarrow 0) = 0$, whereas the gap remains finite in the MI_{am} phase when $g = 0$.

We first use the MFT described in Sec. III A for studying the phase diagram and the quantum phase transitions. Then, we perform exact QMC simulations described in Sec. III B for a more extensive analysis of the quantum phase transitions.

A. Mean-field phase diagram

The atomic-molecular conversions strongly affect the insulating-BEC transition with two particles per site and give rise to an insulating phase at the tip of the $\rho = 2$ Mott lobe. As a reference, for the standard single species Bose-Hubbard model, the Mott-superfluid transition is located at $t_c/U \simeq 0.025$ ($t_c/U \simeq 0.043$) for $\rho = 2$ ($\rho = 1$), according to the mean field method of Sec. III A. Activating the conversion, Fig. 1 shows the atomic and molecular condensate fractions C_a^{MF} and C_m^{MF} as functions of the

hopping t/U in different regions of the detuning. For

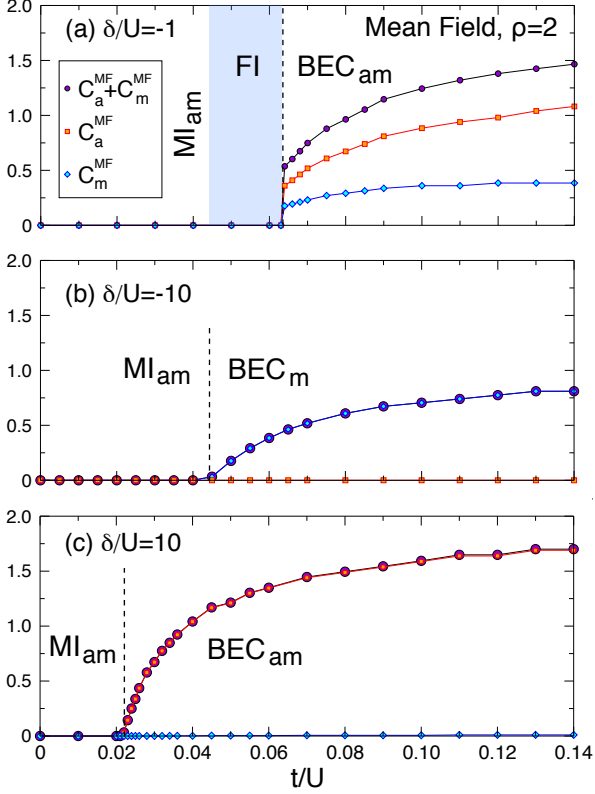


FIG. 1: (Color online) Mean field insulating-BEC transition for fixed density $\rho = 2$ with $g/U = 0.8$ close to the resonance (a) $\delta/U = -1$, (b) on the molecular side $\delta/U = -10$, and (c) on the atomic side $\delta/U = 10$. The FI phase is stabilized by the conversion g whereas the MI_{am} phase is stabilized by the interactions U . The jump in the condensate fractions C_a^{MF} and C_m^{MF} at the FI-BEC_{am} transition indicates a first-order transition, associated with the metastable region $t/U \in]0.061; 0.065[$ where the ground state energy exhibits global and local minima.

small t/U , the system is in a MI_{am} phase for all detuning Fig. 1 (a-c) and the particle-hole gap is stabilized by the interaction U . Three scenarios are observed when the hopping t/U is increased. Firstly, close to the resonance both C_a^{MF} and C_m^{MF} turn on simultaneously and jump at the transition, indicating the existence of a metastable region at the transition and a quantum first-order transition – see Fig. 1 (a). Clearly, the transition takes place at a critical hopping $t_c/U \simeq 0.062$ bigger than the standard critical hopping of the Mott-superfluid transition without conversions $g = 0$ at any filling. Therefore, the interactions U alone cannot open the particle-hole gap at the tip of the insulating lobe, which is rather stabilized by the conversions g : the system is in a FI phase. Secondly, only the molecular condensation $C_m^{MF} \neq 0$ occurs on the molecular side – see Fig. 1 (b) – the atoms being almost eliminated adiabatically for $\delta/U = -10$.

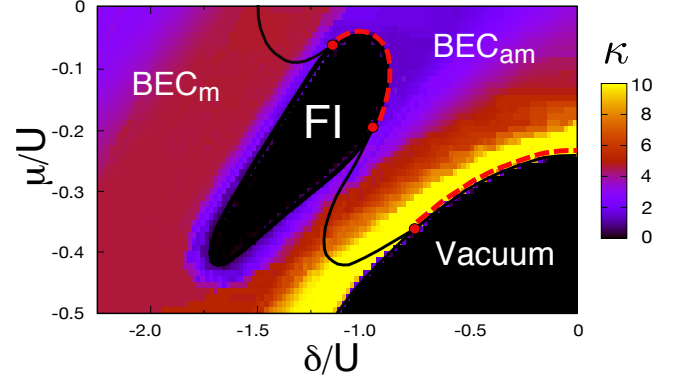


FIG. 2: (Color online) Mean-field ground state phase diagram, taken from Ref. [21], with $t/U = 0.06$ and $g/U = 0.8$ (false colors indicate the compressibility κ Eq. (10)). The following phases appear in the phase diagrams: Feshbach insulator (FI) with $\rho = 2$, molecular (BEC_m) and atomic-molecular (BEC_{am}) condensate. Second-order transitions are denoted by solid black lines, red dashed lines indicate first-order transitions, and red dots denote tricritical points.

Consequently, the transition occurs close to the standard critical value $t_c/U \simeq 0.043$ of the single species Bose-Hubbard model with $\rho_m \sim 1$. Lastly, for $\delta/U = 10$ (Fig. 1 (c)), the system is mainly composed by atoms and a mixed condensation occurs when t/U is increased (the molecular condensate is small but finite). Although we numerically observe a continuous MI_{am} -BEC_{am} transition, a weak first-order transition is not excluded when fluctuations are taken into account. This, however, does not happen, as we discuss in the following.

We now turn our attention to the phase diagram close to the resonance with a fixed hopping $t/U = 0.06$ in order to focus on the FI phase. Figure 2, from Ref. [21], shows the phase diagram as a function of the detuning δ/U and of the chemical potential μ/U . The incompressible region (black region in Fig. 2) reveals the existence of the particle-hole gap of the FI phase with $\rho = 2$. The molecular condensation BEC_m and the mixed condensation BEC_{am} are also observed in the phase diagram. First-order transitions, indicated by red dashed lines in Fig. 2, are systematically observed when both atomic and molecular order parameters are simultaneously turned on, i.e. when the global symmetry of the model $U(1) \times \mathbb{Z}_2$ is destroyed [39]. The first-order nature of the transition is not specific to the transition to the FI, but it appears to be generic for all insulating-BEC_{am} transitions [20]. Although this phase diagram was discussed in Ref. [21], the phase transitions have not yet been properly examined using an exact method.

Changing the detuning δ/U , i.e. the control parameter in the experiment, can drive the system into different phases, leading to quantum phase transitions without changing the hopping parameter t/U . This gives the experimental possibility to observe multiple transitions

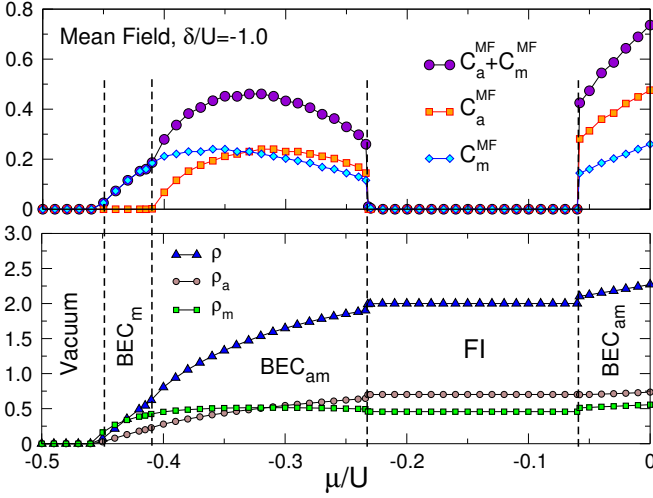


FIG. 3: (Color online) Vertical cut of the mean-field phase diagram in Fig. 2 for $\delta/U = -1.0$. The BEC_{am} -FI transition is first-order whereas the other transitions are continuous.

and more specifically the first-order FI- BEC_{am} transition. The direct observation of the density profile for a fixed detuning would give rise to intriguing shapes since many first-order transitions are involved. According to the local density approximation, the density profile is obtained by a vertical scan of the phase diagram by changing the chemical potential μ/U . Figure 3 shows the condensates and the densities for such a vertical cut with $\delta/U = -1.0$. The system evolves continuously from vacuum to BEC_m and to BEC_{am} when μ/U increases, and all the quantities jump at the first-order BEC_{am} -FI transition. Note that both atomic and molecular densities, ρ_a and ρ_m , reach a noninteger plateau in the FI phase, whereas the total density is integer $\rho = \rho_a + 2\rho_m = 2$.

The mean field analysis reports a rich physics attributed to the conversion term in Eq. (3) but does not allow the classification of the transitions which requires the calculation of the correlation functions.

B. Quantum Monte Carlo simulations

The MFT results are qualitatively confirmed by our QMC simulations. Figure 4 (a) shows that, upon lowering t/U , the atomic and molecular condensates exhibit a clear jump at the tip of the FI, witnessing the first-order nature of the FI- BEC_{am} transition. The jump is also observed in the superfluid density. The transition occurs at a critical $t_c/U \simeq 0.076$ value well above the standard critical hopping of the MI-SF transition without conversions $g = 0$ at any filling (e.g. $t_c/U \simeq 0.059$ for the single-species Bose-Hubbard model at the MI-SF transition with $\rho = 1$ [40]), then proving the crucial contribution of the conversions in the particle-hole gap stabilization. The MI_{am} -FI crossover was investigated in

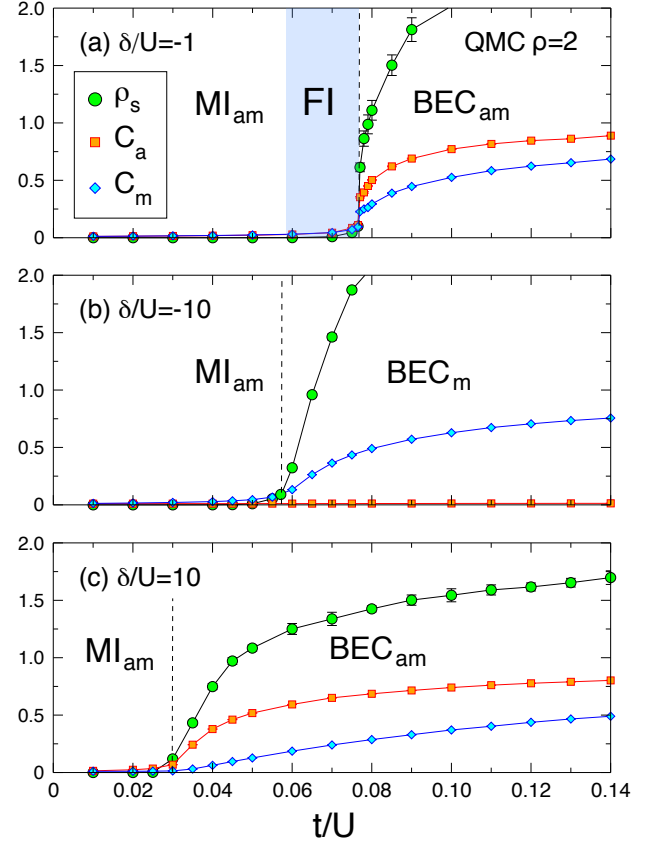


FIG. 4: (Color online) QMC simulations of the insulating-BEC transition with $L = 10$ for fixed density $\rho = 2$ and $g/U = 0.6$, $\beta t = 20$ close to the resonance (a) $\delta/U = -1$, (b) on the molecular side $\delta/U = -10$, and (c) on the atomic side $\delta/U = 10$. These results are in good qualitative agreement with the mean field predictions of Fig. 1. (a) Close to the resonance, the conversion stabilizes the FI phase. The discontinuities in the atomic and molecular condensates, C_a and C_m (Eq. 11), and in the superfluid density ρ_s (Eq. 12), indicate a first-order transition.

Ref. [21]. Far on the molecular side – Fig. 4 (b) – only the molecular condensation occurs, and the continuous MI_{am} - BEC_m transition takes place close to $t_c/U \simeq 0.054$. Finally, on the atomic side – Fig. 4 (c) – we do not observe a jump at the MI_{am} - BEC_{am} transition at $t_c/U \simeq 0.03$.

To confirm the presence of a first-order quantum phase transition near the tip of the FI lobe, we perform a finite size analysis of the condensates C_a , C_m and of the superfluid density ρ_s . Indeed, since the correlation length does not diverge at a first-order transition, the jump should increase with the system size for small systems, and then saturate for big sizes. Figure 5 clearly shows that the jump increases with the linear system size L , indicating a first-order FI- BEC_{am} phase transition. This conclusion is strengthened by QMC grand canonical simulations, see Fig. 6, where the density jumps at the FI- BEC_{am} transition indicating a metastable region and a first-order tran-

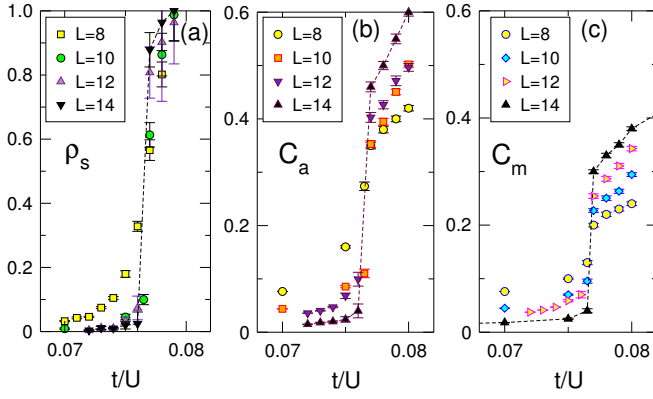


FIG. 5: (Color online) Finite size analysis of the (a) superfluid density ρ_s and of the condensates (b) C_a and (c) C_m at the FI-BEC_{am} transition using QMC simulations with $\delta/U = -1$, $g/U = 0.6$, $\beta t = 2L$ and $\rho = 2$ for linear sizes $L = 8, 10, 12, 14$. The jump at the transition increases with L .

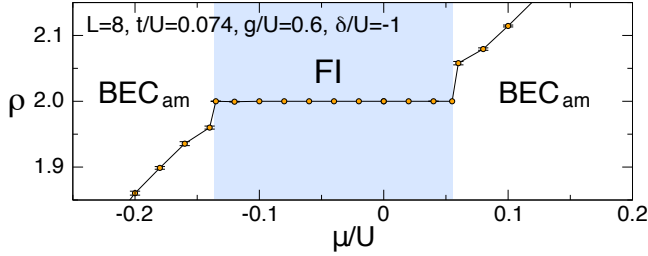


FIG. 6: (Color online) QMC grand canonical simulations for $L = 8$ and the same other parameters as in Fig. 5. The density ρ is discontinuous at the FI-BEC_{am} transition.

sition at the tip of the FI lobe.

We now investigate the quantum phase transitions keeping both hopping and conversion fixed and varying the detuning δ/U . Since the FI phase is stabilized for even densities only, two different behaviors are observed for even and odd densities. We first discuss the case with two particles per site. Starting in the BEC_m phase for large negative δ/U , the system evolves firstly in the FI phase, and then in the BEC_{am} phase when increasing the detuning – see Fig. 7. As expected, the atomic density ρ_a increases with the detuning, see Fig. 7 (a) and both atomic and molecular densities jump at the first-order FI-BEC_{am} transition, see inset Fig. 7 (a). This jump is also clearly observed in the superfluid density and in the condensate fractions at the FI-BEC_{am} transition (Fig. 7 (b-d)).

As shown in Fig. 8, the FI phase cannot be stabilized for $\rho = 1$ and a BEC_m-BEC_{am} transition is induced upon increasing the detuning δ/U . This transition, captured also at the mean-field level, is related to the breaking of the \mathbb{Z}_2 symmetry associated with the phase of the atomic field, and it is therefore expected to belong to the 3D

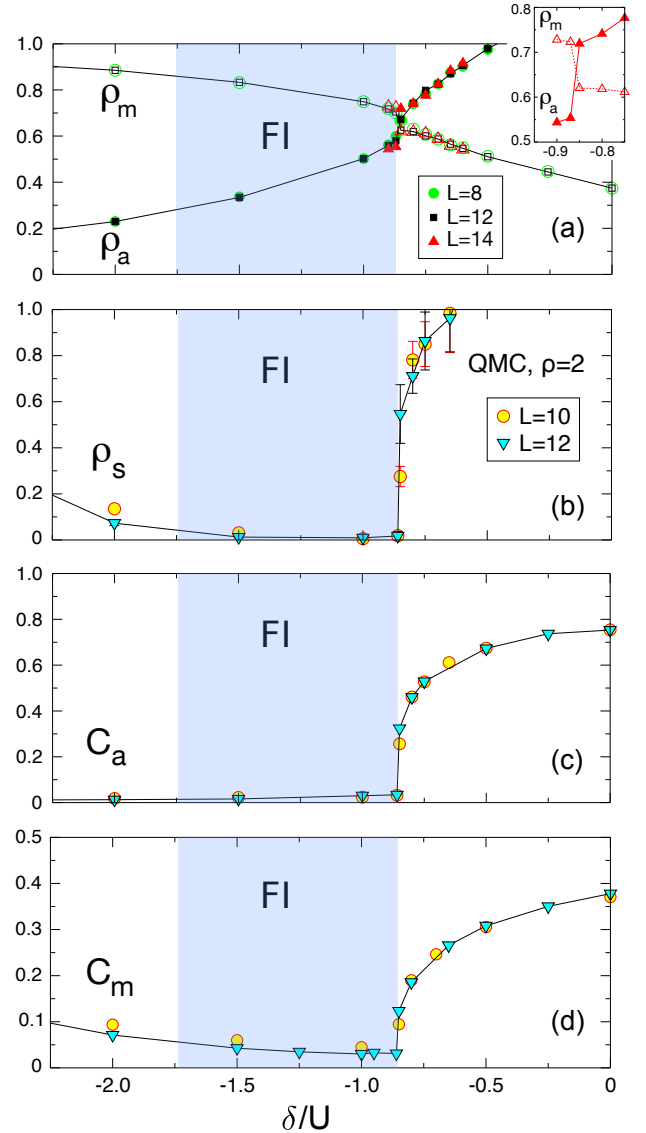


FIG. 7: (Color online) QMC canonical simulations at fixed total density $\rho = 2$, with $g/U = 0.6$, $\beta t = 2L$ and $t/U = 0.07$. (a) Atomic ρ_a and molecular ρ_m densities as functions of detuning: both densities jump at the first-order FI-BEC_{am} transition (see zoom in inset for $L = 14$); A jump is also observed in the (b) superfluid density ρ_s , as well as in the (c) atomic C_a and (d) molecular C_m condensates when the size of the system increases.

Ising universality class. While the universality class cannot be correctly reproduced at the mean-field level, our QMC simulations show a very convincing scaling of the condensate fraction as $C_a = L^{-2\beta/\nu} f(L^{1/\nu}|\delta - \delta_c|/U)$ with exponents β and ν belonging to the 3D Ising universality class – see Fig. 9 (b) for $\rho = 1$. The BEC_m-BEC_{am} transition also belongs to the 3D Ising universality class for $\rho \neq 1$ according to our QMC simulations – e.g. see Fig. 9 (a) for $\rho = 0.5$. Similarly to the single-

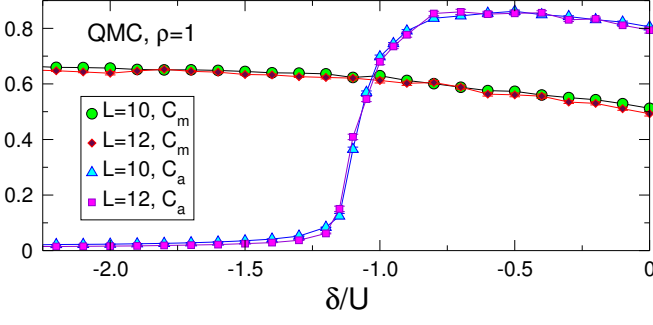


FIG. 8: (Color online) QMC canonical simulations of the atomic and molecular condensates as functions of the detuning δ/U for $\rho = 1$, $g/U = 0.6$, $t/U = 0.07$, and $\beta t = 2L$ and two linear sizes $L = 10$ and $L = 12$. The system evolves from a BEC_m to a BEC_{am} phase when increasing the detuning δ/U .

Quantum Phase Transition	Order	Universality Class
$\text{BEC}_m\text{-BEC}_{am}$	2 nd	3D Ising
$\text{BEC}_m\text{-FI } \rho = 2$	2 nd	3D XY
$\text{BEC}_m\text{-FI } \rho \neq 2$	2 nd	Mean field
Vacuum- BEC_m	2 nd	Mean field
Vacuum- BEC_{am}	1 st	\emptyset
FI- BEC_{am}	1 st	\emptyset

TABLE I: Order and universality class of the quantum phase transitions of the phase diagram Fig. 2.

species Bose-Hubbard model, the scaling of C_m is found to be consistent with the 3D XY universality class at the $\rho = 2$ $\text{BEC}_m\text{-FI}$ transition where only the U(1) symmetry is spontaneously restored – see Fig. 9 (b). The other transitions in the phase diagram of Fig. 2, i.e. vacuum- BEC_m and FI- BEC_m with $\rho \neq 2$, are second order (not shown). The order and the universality class of the quantum phase transitions of the phase diagram in Fig. 2 are summarized in Table I.

V. THERMAL PHASE DIAGRAM

In two dimensions, the Bose-Einstein condensation at finite temperature is impossible in the proper sense [41], leaving space to quasicondensation via a BKT transition [27], associated with the unbinding transition of pairs of topological excitations (vortices and antivortices). In this context, the coherent coupling between atoms and molecules establishes a correlation among the topological defects in the phase patterns of both species which brings interesting features [28]. We first analyze the thermal phase diagram for $\rho = 2$, and then turn to an analysis of the thermal phase transitions.

A. Thermal phase diagram for $\rho = 2$

The ground state analysis (Sec. IV) revealed the possibility to stabilize an insulating phase, the FI phase, with a finite particle-hole gap opened by the conversions between atoms and molecules for even total density. The FI phase evolves either in a BEC_m phase when decreasing the detuning δ , or in a mixed BEC_{am} phase when increasing δ (see Fig. 7). The thermal phase diagram, plotted in Fig. 10, shows the evolution of the phases when activating the thermal effects. As expected, the molecular (mixed) condensate become molecular (mixed) superfluid at low temperature with $\rho_s \neq 0$ and the system is in a normal Bose liquid (NBL) at high temperature for all detuning δ . The critical temperature at the SF-NBL transition is determined using finite size analysis, see Sec. VB.

Note that the mixed superfluid SF_{am} and the molecular superfluid SF_m , separated by the FI phase at $T = 0$, remain well separated for all temperature and the in-

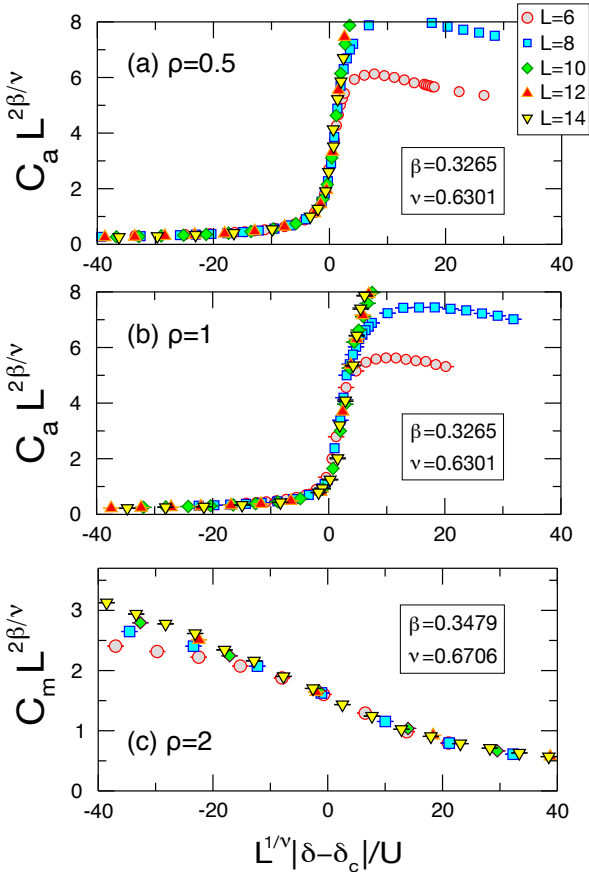


FIG. 9: (Color online) Scaling plots of the atomic and molecular condensates for the quantum phase transition from BEC_m to BEC_{am} with (a) $\rho = 0.5$, (b) $\rho = 1$, and (c) from BEC_m to FI with $\rho = 2$, as obtained via QMC simulations with $\beta t = 2L$. Critical exponents of the (a-b) 3D Ising and (c) 3D XY universality classes [42], cited in the boxes, are used for the scaling.

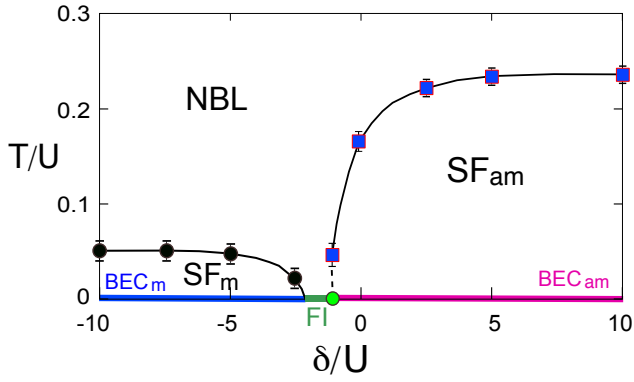


FIG. 10: (Color online) QMC thermal phase diagram with $\rho = 2$, $g/U = 0.6$ and $t/U = 0.07$: the BEC phases existing strictly at $T = 0$ become superfluid (SF) and then normal Bose liquid (NBL) when heating the system, keeping the detuning constant, whereas the FI phase crossed over the NBL phase. Black circles and blue squares are obtained using finite size scaling analysis, see respectively Figs. 12 and 13. The green point indicates a quantum first-order transition; the dashed line indicates a possible first-order transition.

ulating FI phase crossed over the NBL phase when the temperature is increased. Interestingly, although $t_a = t_m = t$, the SF_{am} phase is more robust with respect to the thermal effects, compared to the single component SF_m superfluid. This can be qualitatively explained by looking at the atomic (molecular) characteristic interacting scales $J_{a(m)} \sim \rho_{a(m)}t$, where $\rho_a = 2$ far on the atomic side ($\delta \rightarrow +\infty$) and $\rho_m = 1$ far on the molecular side ($\delta \rightarrow -\infty$). Therefore, the interacting scale in the SF_{am} phase is twice as large as the one in the SF_m phase. The same behavior has been observed at the mean field level in 3D [18].

B. Quantum-to-classical first-order phase transition and nonconventional BKT transitions

The quantum first-order transition between the FI and the mixed condensate BEC_{am} requires a specific attention since it is not excluded that the metastability region persists at $T \neq 0$. Indeed, the discontinuity in the superfluid density at the disordered- SF_{am} transition – discontinuity associated with the existence of the metastability region – persists at finite temperature, see Fig. 11 (a). Interestingly enough, the discontinuity in ρ_s observed at $T/U = 0.035$ in Fig. 11 (a) – a temperature close to the critical temperature of the SF_m -NBL transition far on the molecular side, reinforces the idea that the quantum first-order FI- BEC_{am} transition becomes a classical first-order NBL- SF_{am} transition. As previously discussed, the discontinuity in ρ_s increases with the system size at a first-order transition. This behavior is clearly observed for $T/U = 0.035$ in Fig. 11 (a). However, we do not ob-

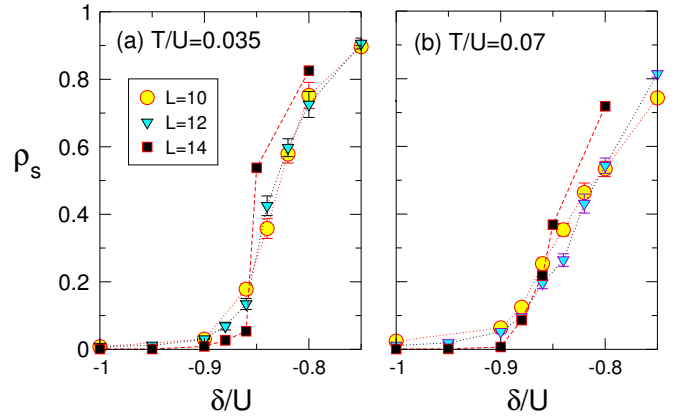


FIG. 11: (Color online) Superfluid density as a function of the detuning at the $\rho = 2$ disordered- SF_{am} transition for finite temperatures with $L = 10, 12, 14$, $g/U = 0.6$ and $t/U = 0.07$. The discontinuity in ρ_s , observed for (a) $T/U = 0.035$, decreases with the temperature. No jump is observed for (b) $T/U = 0.07$.

serve other clear signals of a first-order transition (two-peak structures in histograms or negative compressibility) and therefore we are not able to discern whether the phase transition indeed is first order or not.

We now concentrate on vertical slices of the phase diagram in Fig. 10, starting in the condensed phase at low temperature, keeping the detuning fixed and varying the temperature. It is well known that the loss of the quasi-long-range coherence at a BKT transition is associated with the unbinding of vortices and antivortices and with a scaling of the quasicondensate such that $C \propto L^{-\eta}$ with the critical exponent $\eta(T_{BKT}) = 1/4$ [43]. Furthermore, the superfluid density satisfies the universal jump $\rho_s/T_{BKT} = 2/\pi$ at the transition [44]. To avoid any confusion, we stress that the universal jump in ρ_s at a BKT transition is only observed in the thermodynamic limit (e.g., see Fig. 12 (b)), and therefore cannot be confused with the discontinuity at a first-order transition observed for $L \sim 10$. In the case of coupled fields, the BKT transition implies a more complex mechanism since the topological defects are coupled, as for e.g., unbinding of half-vortices instead of the usual integer vortices [28, 45–47].

We first discuss the BKT transition far on the molecular side, with $\delta/U = -10$ – see Fig. 12. The critical temperature $T_{BKT}/U \sim 0.045$, in agreement with Ref. [40], is determined from the finite size scaling of the molecular condensate fraction $C_m(T_{BKT}) \propto L^{-1/4}$ with system sizes up to $L = 14$ – see Fig. 12 (a). Moreover, the BKT transition is found to be consistent with an anomalous $8T_{BKT}/\pi$ stiffness jump at T_{BKT} instead of $2T_{BKT}/\pi$ – see Fig. 12 (b). This anomalous jump is easily understood by rewriting the superfluid density Eq. (12) with a vanishing atomic winding number $\langle W_a \rangle = 0$ on the molecular side, leading to $\rho_s = \frac{\langle (2W_m)^2 \rangle}{4t\beta} = 4\rho_{s0}$, with

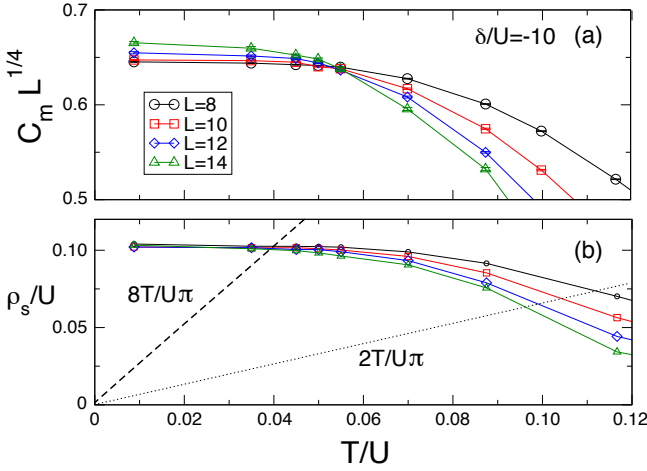


FIG. 12: (Color online) (a) Scaling of the molecular condensate C_m and (b) superfluid density as functions of temperature for different sizes and $\rho = 2$, $g/U = 0.6$, $t/U = 0.07$, and $\delta/U = -10$. The critical temperature extracted from scaling analysis with the BKT exponent in (a) is consistent with an anomalous $8T_{BKT}/\pi$ stiffness jump instead of $2T_{BKT}/\pi$.

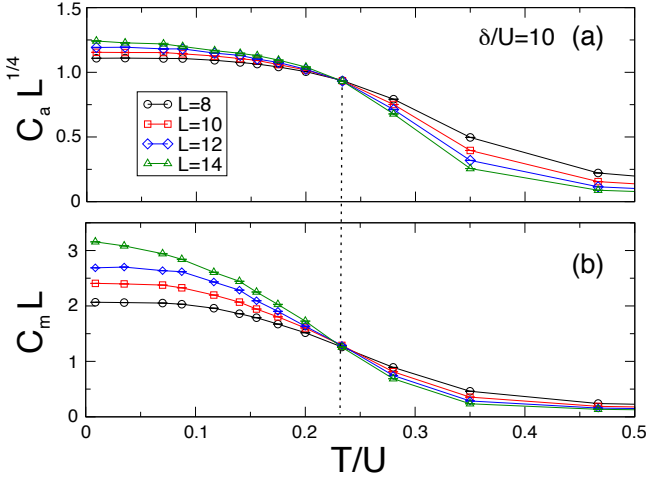


FIG. 13: (Color online) Scaling of the (a) atomic and (b) molecular condensate as functions of temperature for different sizes with $\rho = 2$, $g/U = 0.6$, $t/U = 0.07$, and $\delta/U = 10$.

ρ_{s0} the single component winding number. That immediately gives the factor 4 involved in the anomalous stiffness jump observed.

On the atomic side, the situation is more complex since both atomic and molecular fields are coupled in a regime of a quasi-long range order in their correlation. For large positive detuning, we expect the atomic condensate fraction C_a to satisfy the standard BKT scaling. This behavior is depicted for $\delta/U = 10$ in Fig. 13 (a), where $C_a(T_{BKT}) \propto L^{-1/4}$. This transition is in agreement with the standard $2T_{BKT}/\pi$ universal stiffness jump (not

Thermal Phase Transition	Type
SF _m -NBL	BKT with anomalous $8T_{BKT}/\pi$ jump in ρ_s
SF _{am} -NBL (low temperature)	Possible 1 st order
SF _{am} -NBL	Normal atomic BKT with $\eta_a(T_{BKT}) = 1/4$, Abnormal molecular BKT with $\eta_m(T_{BKT}) = 1$

TABLE II: Order and universality class of the thermal phase transitions of the phase diagram in Fig. 10.

shown). As discussed in Sec. IV for $T = 0$, the molecular phase ϕ_r^m is locked (from the mean field point of view) to the nonzero value acquired by the phase of atomic pairs $\langle e^{i2\phi_r^a} \rangle$, since the average phase of the atoms acquires a finite value $\langle e^{i\phi_r^a} \rangle \neq 0$. As a consequence, the topological defects in the atomic and molecular field are coupled also at finite temperature, leading to the appearance of vortices in the molecular field due to the conversion term [28]. For large coupling, the molecular field is expected to quasicondense at the atomic BKT transition in the same way as atom pairs condense. Therefore, the molecular BKT transition, driven by the atomic-pair field dynamics, does not satisfy the normal BKT scaling $C_m(T_{BKT}) \propto L^{-1/4}$ but satisfies the scaling of the atom-pair such that $C_m(T_{BKT}) \propto L^{-1}$ as shown in Fig. 13 (b). This result is in good agreement with a previous study of an effective XY coupled model [28]. Therefore, the fact that both atomic and molecular BKT transitions occur at the same critical temperature $T_{BKT}/U \simeq 0.23$, see Fig. 13, indicates that the molecular field mimics the behavior of the atomic pairs exactly, or in other words $g/U = 0.6$ is a strong coupling. The order and the universality class of the thermal phase transitions of the phase diagram in Fig. 10 are summarized in Table II.

VI. CONCLUSION

Studying numerically a coherently coupled 2D atom-molecule mixture at zero and finite temperature, we unveiled the phase diagram and the universal traits of the transitions. At zero temperature, we have shown that an insulating phase is stabilized close to the Feshbach resonance – the Feshbach insulator – by the atom-molecule conversion term in a region where interactions alone cannot stabilize a Mott insulator. The Feshbach insulator involved noninteger density plateaus for both atomic and molecular species such that $\rho_a \sim 2\rho_m$ close to the resonance. Such a measurement, directly accessible using Stern-Gerlach separation during the cloud expansion [48], will be a definitive evidence that this phase is not a standard Mott phase with integer density. The ground state phase diagram comprises the FI phase close to the resonance, a molecular condensate

for negative detuning, and a mixed atomic-molecular condensate for positive detuning. The richness of the phase diagram also comes from the variety of quantum phase transitions: the transition from molecular to mixed condensate is found to be of the 3D Ising type due to the breaking of the \mathbb{Z}_2 symmetry associated with the phase of the atomic field; the transition from molecular condensate to Feshbach insulator belongs to the universality class of the 3D XY model; and interestingly enough, the transition from mixed condensate to disordered phase (vacuum or Feshbach insulator) associated with the spontaneous symmetry breaking of both U(1) and \mathbb{Z}_2 is systematically found to be of the first order; otherwise the transitions are second order. The thermal effects are also discussed. The conversion term couples coherently and asymmetrically the phase of the atomic and molecular fields, and therefore strongly affects the BKT transition. This leads to an unusual molecular superfluid to normal Bose liquid BKT transition, involving a renormalized $8T_{BKT}/\pi$ stiffness jump, instead of the standard $2T_{BKT}/\pi$ one for the single component case. The transition from mixed superfluid

to normal Bose liquid also requires a careful treatment since only the atomic BKT transition is conventional whereas the thermal disintegration of the molecular superfluid satisfies the scaling of the atom-pair such that $C_m(T_{BKT}) \propto L^{-1}$. Finally, we observe a discontinuity in the superfluid density at the mixed superfluid to normal Bose liquid transition, indicating the existence of a possible classical first-order transition. These rich phenomena are amenable to experimental verification using state-of-the-art setups in cold-atom physics.

Acknowledgements. We thank T. Roscilde, F. Hébert, and A. Rançon for useful discussions and for their critical reading of the manuscript. We also thank Professor Min-Fong Yang for critical comments and suggestions. L.dF.dP also thanks Sasha de Forges de Parny and Solenne Ghintran for their support. This work is supported by Agence Nationale de la Recherche (“ArtiQ” project) and the Alexander von Humboldt-Foundation. All calculations have been performed on the PSMN center of the ENS-Lyon.

-
- [1] I. Bloch, J. Dalibard, and W. Zwerger, *Rev. Mod. Phys.* **80**, **885** (2008).
 - [2] *Quantum Phase Transitions*, S. Sachdev (Cambridge University Press, 1999).
 - [3] M. Greiner, O. Mandel, T. Esslinger, T. W. Hänsch, and I. Bloch, *Nature* **415**, 39 (2002).
 - [4] C. Chin, R. Grimm, P. Julienne, and E. Tiesinga, *Rev. Mod. Phys.* **82**, 1225 (2010).
 - [5] M. Greiner, C. A. Regal, and D. S. Jin, *Nature* **426**, 537 (2003).
 - [6] M. Randeria and E. Taylor, *Ann. Rev. Cond. Matt.* **5**, 209 (2014).
 - [7] W. Ketterle and M. W. Zwierlein, in *Ultracold Fermi Gases, Proceedings of the International School of Physics “Enrico Fermi”, Course CLXIV*, M. Inguscio, W. Ketterle, and C. Salomon (eds.), IOS Press, Amsterdam, 2008.
 - [8] K. Winkler, G. Thalhammer, F. Lang, R. Grimm, J. Hecker Denschlag, A. J. Daley, A. Kantian, H. P. Büchler, and P. Zoller, *Nature* **441**, 853 (2006).
 - [9] S. Inouye, M. R. Andrews, J. Stenger, H.-J. Miesner, D. M. Stamper-Kurn, and W. Ketterle, *Nature* **392**, 151 (1998).
 - [10] E. A. Donley, N. R. Claussen, S. T. Thompson, and C. E. Wieman, *Nature* **417**, 529 (2002).
 - [11] J. Stenger, S. Inouye, M. R. Andrews, H.-J. Miesner, D. M. Stamper-Kurn, and W. Ketterle, *Phys. Rev. Lett.* **82**, 2422 (1999).
 - [12] R. Jördens, N. Strohmaier, K. Günter, H. Moritz, and T. Esslinger, *Nature* **455**, 204 (2008).
 - [13] B. Deissler, M. Zaccanti, G. Roati, C. D’Errico, M. Fattori, M. Modugno, G. Modugno, and M. Inguscio, *Nature Phys.* **6**, 354 (2010).
 - [14] N. Syassen, D. M. Bauer, M. Lettner, D. Dietze, T. Volz, S. Dürr, and G. Rempe, *Phys. Rev. Lett.* **99**, 033201 (2007).
 - [15] Th. Busch, B.-G. Englert, K. Rzazewski, and M. Wilkens, *Found. Phys.* **28**, 549 (1998).
 - [16] M. L. Olsen, J. D. Perreault, T. D. Cumby, and D. S. Jin, *Phys. Rev. A* **80**, 030701(R) (2009).
 - [17] K. Sengupta and N. Dupuis, *Europhys. Lett.* **70**, 586 (2005).
 - [18] L. Radzihovsky, J. I. Park, and P. B. Weichman, *Phys. Rev. Lett.* **92**, 160402 (2004).
 - [19] M. W. J. Romans, R. A. Duine, S. Sachdev, and H. T. C. Stoof, *Phys. Rev. Lett.* **93**, 020405 (2004).
 - [20] L. Radzihovsky, P. B. Weichman, and J. I. Park, *Ann. Phys.* **323**, 2376 (2008).
 - [21] L. de Forges de Parny, V. G. Rousseau, and T. Roscilde, *Phys. Rev. Lett.* **114**, 195302 (2015).
 - [22] S. Capponi, G. Roux, P. Azaria, E. Boulat, and P. Lecheminant, *Phys. Rev. B* **75**, 100503(R) (2007).
 - [23] G. Roux, S. Capponi, P. Lecheminant, and P. Azaria, *Eur. Phys. J. B* **68**, 293 (2009).
 - [24] S. Ejima, M. J. Bhaseen, M. Hohenadler, F. H. L. Essler, H. Fehske, and B. D. Simons, *Phys. Rev. Lett.* **106**, 015303 (2011).
 - [25] M. J. Bhaseen, S. Ejima, F. H. L. Essler, H. Fehske, M. Hohenadler, and B. D. Simons, *Phys. Rev. A* **85**, 033636 (2012).
 - [26] N. F. Mott and R. Peierls, *Proceedings of the Physical Society*, vol. 49, no. 4S, pp. 72-73, 1937.
 - [27] J. V. José (Ed.), *40 Years of Berezinskii-Kosterlitz-Thouless Theory*, World Scientific, 2013.
 - [28] L. de Forges de Parny, A. Rançon, and T. Roscilde, *Phys. Rev. A* **93**, 023639 (2016).
 - [29] D. B. M. Dickerscheid, U. Al Khawaja, D. van Oosten, and H. T. C. Stoof, *Phys. Rev. A* **71**, 043604 (2005).
 - [30] T. Köhler, K. Góral, and P. S. Julienne, *Rev. Mod. Phys.* **78**, 1311 (2006).

- [31] V. G. Rousseau and P. J. H. Denteneer, Phys. Rev. A **77**, 013609 (2008); V. G. Rousseau and P. J. H. Denteneer, Phys. Rev. Lett. **102**, 015301 (2009).
- [32] M. Eckholt and T. Roscilde, Phys. Rev. Lett. **105**, 199603 (2010).
- [33] V.G. Rousseau, Phys. Rev. E **77**, 056705 (2008).
- [34] V.G. Rousseau, Phys. Rev. E **78**, 056707 (2008).
- [35] L. de Forges de Parny, F. Hébert, V. G. Rousseau, R. T. Scalettar, and G. G. Batrouni, Phys. Rev. B **84**, 064529 (2011).
- [36] L. de Forges de Parny, F. Hébert, V. G. Rousseau, and G. G. Batrouni, Phys. Rev. B **88**, 104509 (2013).
- [37] L. de Forges de Parny, F. Hébert, V. G. Rousseau, and G. G. Batrouni, Eur. Phys. J. B **85**, 169 (2012).
- [38] D.M. Ceperley and E.L. Pollock, Phys. Rev. **B39**, 2084 (1984).
- [39] Interestingly, first-order transitions are generically found in three dimensions when the breaking of a $U(1) \times \mathbb{Z}_2$ symmetry is involved. See for instance: V. Thanh Ngo and H. T. Diep, J. Appl. Phys. **103**, 07C712 (2008); A. O. Sorokin, JETP **118**, 417 (2014).
- [40] B. Capogrosso-Sansone, N. V. Prokof'ev, and B. V. Svistunov, Phys. Rev. A **77**, 015602 (2008).
- [41] P. C. Hohenberg, Phys. Rev. **158**, 383 (1967); N. D. Mermin, Phys. Rev. **176**, 250 (1968); N. D. Mermin and H. Wagner, Phys. Rev. Lett. **17**, 1133 (1966).
- [42] A. Pelissetto and E. Vicari, Phys. Rep. **368**, 549 (2002).
- [43] M. Le Bellac, *"Quantum and Statistical Field Theory"*, Oxford University Press (1992).
- [44] D.R. Nelson, and J. M. Kosterlitz, Phys. Rev. Lett. **39**, 1201 (1977).
- [45] S. Mukerjee, C. Xu and J.E. Moore, Phys. Rev. Lett. **97**, 120406 (2006).
- [46] L. Bonnes, and S. Wessel, Phys. Rev. Lett. **106**, 185302 (2011).
- [47] K.-K. Ng, and M.-F. Yang, Phys. Rev. B **83**, 100511 (2011).
- [48] J. Herbig, T. Kraemer, M. Mark, T. Weber, C. Chin, H.-C. Nägerl, and R. Grimm, Science **301**, 1510 (2003).